PAPER

Engineering of functional, perfusable 3D microvascular networks on a chip†

Sudong Kim,[a] Hyunjae Lee,[b] Minhwan Chung[a] and Noo Li Jeon*[abc]

Generating perfusable 3D microvessels *in vitro* is an important goal for tissue engineering, as well as for reliable modelling of blood vessel function. To date, *in vitro* blood vessel models have not been able to accurately reproduce the dynamics and responses of endothelial cells to grow perfusable and functional 3D vascular networks. Here we describe a microfluidic-based platform whereby we model natural cellular programs found during normal development and angiogenesis to form perfusable networks of intact 3D microvessels as well as tumor vasculatures based on the spatially controlled co-culture of endothelial cells with stromal fibroblasts, pericytes or cancer cells. The microvessels possess the characteristic morphological and biochemical markers of *in vivo* blood vessels, and exhibit strong barrier function and long-term stability. An open, unobstructed microvasculature allows the delivery of nutrients, chemical compounds, biomolecules and cell suspensions, as well as flow-induced mechanical stimuli into the luminal space of the endothelium, and exhibits faithful responses to physiological shear stress as demonstrated by cytoskeleton rearrangement and increased nitric oxide synthesis. This simple and versatile platform provides a wide range of applications in vascular physiology studies as well as in developing vascularized organ-on-a-chip and human disease models for pharmaceutical screening.

Introduction

The circulatory system is constructed from a network of blood vessels, which mediate a wide range of functions including cellular and biochemical transport, nutrient and oxygen exchange, and temperature regulation, while maintaining a high degree of plasticity throughout the life of an organism. The foundation of this system is vascular endothelial cells (ECs), the building blocks which regulate transvascular transport, vasodilation, and vessel formation and regression. As with any system of such complexity, malfunction and dysregulation can lead to a multitude of pathologies,[1] thus engineering blood vessels *in vitro* is an important tool for the discovery of drugs and therapeutics to treat such pathologies.

Toward this goal, there are numerous reports of *in vitro* experimental systems developed to investigate vessel dynamics and function. For example, ECs cultured on 2D glass substrates or porous membranes are widely used for the investigation of barrier function,[2] mechanosensitive response of the endothelium,[3] and transendothelial migration of blood-borne cells including leukocytes[4] and circulating tumor cells (CTCs).[5] However, such 2D monolayer-based systems lack three-dimensional contexts important for the native architectures and functions of blood vessels,[6,7] thus failing to reflect biological complexities found in real organisms.

In contrast, three-dimensional extracellular matrices (ECMs) can provide an enhanced environment for multicellular organization of ECs as well as cell–cell and cell–matrix interactions, all of which have been shown to be critical in endothelial morphogenesis and function.[8,9] However, conventional 3D *in vitro* models have not provided a robust experimental method to grow readily perfusable blood vessels, precluding their use in the experiments requiring selective delivery of small molecules, soluble proteins or cell suspensions to the luminal surface of the endothelium. Furthermore, the resulting cellular microenvironments in these models do not capture key mechanical cues defined by luminal flow which play central roles in the modulation of endothelial functions.

Recent reports, assisted by micro-technology, demonstrated *in vitro* perfusable vessel analogues made by endothelialization of channel-molded hydrogels or microfluidic channels to mimic endothelial cell migration, vascular barrier function, inflammatory response, thrombosis and tumor cell intravasation under defined biomolecular and mechanical stimulations.[10–16] Unfortunately, as these vessels did not follow natural endothelial morphogenesis in making the lumenized structure, they were limited in their ability to reconstitute the

[a] *School of Mechanical and Aerospace Engineering, Seoul National University, Seoul, 151-744, Korea. E-mail: njeon@snu.ac.kr; Tel: +82-2-880-7111*
[b] *Division of WCU Multiscale Mechanical Design, School of Mechanical and Aerospace Engineering, Seoul National University, Seoul 151-744, Korea*
[c] *School of Mechanical and Aerospace Engineering/Seoul National University Institute of Advanced Machinery and Design (SNU-IAMD), Seoul, 151-744, Korea*
† Electronic supplementary information (ESI) available: See DOI: 10.1039/c3lc41320a

characteristic features and responses of *in vivo* endothelia. Several microfluidic approaches have made important progress toward the formation of 3D endothelial tubes *via* physiologically relevant processes.[17–23] Nonetheless, these approaches still fail to provide a practical methodology that closely emulates complex endothelial dynamics to grow native 3D vascular networks which encompass readily perfusable lumina, intact barrier properties, and physiological functions defined by biomechanical stimuli.

Here we report a novel microfluidic platform and robust approach to form perfusable and functional microvascular networks in 3D ECM constructs. The approach uses flexibly designed cellular co-cultures to facilitate controlled heterotypic cell–cell interactions, which reproduces the physiological morphogenesis of ECs to form interconnected networks of microvessels. We have successfully demonstrated that the formation of microvascular networks and the establishment of perfusable lumina are spontaneously directed by ECs and reproduced in a robust manner. The open, long-lasting microvascular networks replicate important features of living vasculatures including native 3D vascular architectures, characteristic biochemical markers, intact barrier function and patent lumina that support luminal flow. In particular, the application of physiological shear stress induced F-actin rearrangement and nitric oxide production in ECs, suggesting that our system efficiently combines important vessel-specific responses and functions in physiologically relevant 3D contexts.

Materials and methods

Device fabrication

Microfluidic devices were fabricated out of polydimethylsiloxane (PDMS, Sylgard 184, Dow Corning) using soft lithography and replica molding. A master with positive relief patterns of photoresist, SU-8 (MicroChem), on a silicon wafer was prepared by photo-lithography. A PDMS prepolymer made of a 10 : 1 (w/w) mixture of PDMS base and curing agent was cast against the master and thermally cured to obtain a negative replica-molded piece. After separation from the master, hydrogel injection ports and the reservoirs for the cell culture medium were punched out of the molded PDMS with a sharpened 18 gauge blunt hypodermic needle and a 6 mm biopsy punch. The PDMS devices and glass coverslips were cleaned with residue-free tape and nitrogen gas air gun, and then treated with oxygen plasma for 45 s to form covalent bonding between them. To restore hydrophobicity to the PDMS after plasma treatment, the devices were kept in an 80 °C dry oven for at least 24 h and sterilized by UV irradiation before each experiment.

Cell culture

Human umbilical vein endothelial cells (HUVEC, Lonza) were cultured in Endothelial Growth Medium (EGM-2, Lonza) and passages 3 to 5 used for experiments. Normal human lung fibroblasts (LF, Lonza) were cultured up to passage 10 in

Fibroblast Growth Medium (FGM-2, Lonza). Cell cultures were grown to 80% confluence prior to passage or use in experiments. Human promyelocytic leukemia cells, HL-60 (a gift from Dr Sunghoon Kim at Seoul National University), were cultured in RPMI-1640 (Hyclone, USA) supplemented with 10% fetal bovine serum, penicillin (100 U/ml), streptomycin (100 U/ml) and HEPES (25 mM). For the investigation of inflammatory response-mediated HL-60 adhesion inside the vessels, HL-60 cells were differentiated over 5 to 7 days in a culture medium containing 1.3% DMSO (Sigma, USA), at an initial concentration of 2×10^5 cells ml^{-1}. Human glioblastoma multiforme cells, U87MG (a gift from Dr Sun Ha Paek at Seoul National University), were cultured in DMEM supplemented with 10% FBS, penicillin (100 U/ml) and streptomycin (100 U/ml). All cells were maintained in a humidified incubator at 37 °C and 5% CO$_2$.

Vasculogenesis cell seeding

The fibrinogen solution was prepared by dissolving 2.5 mg ml^{-1} bovine fibrinogen (Sigma) in DPBS (Gibco) and supplementing aprotinin (0.15 U/ml, Sigma) and collagen type I (0.2 mg ml^{-1}, BD bioscience) to the solution. Collagen type I was added to the pure fibrin matrix to enhance lumen formation of developing tubular structures.[24] After disassociation from culture dishes using 0.25% Trypsin-EDTA (Hyclone), HUVECs and LFs were suspended in the fibrinogen solution, at a concentration of 2 or 3×10^6 cells ml^{-1} for HUVECs and 5×10^6 cells ml^{-1} for LFs. The cell solutions were mixed with thrombin (0.5 U/ml, Sigma) and then immediately introduced into a central channel and stromal cell culture channels (LO, RO). The cell-suspended gel constructs were allowed to clot for 5 min at room temperature. The inlet reservoirs of the cell culture medium channels (LI, RI) were loaded with EGM-2 medium, and then vacuum was applied at the outlet reservoirs to fill the hydrophobic channels. Following loading all four reservoirs, the microfluidic platforms were incubated at 37 °C and 5% CO$_2$. The cell culture medium was removed and refilled with fresh EGM-2 culture medium every 24 h.

Angiogenesis cell seeding

LFs were dissociated from culture dishes and resuspended in a 2.5 mg ml^{-1} bovine fibrinogen solution (2.5 mg ml^{-1} fibrinogen, 0.15 U/ml aprotinin, 0.2 mg ml^{-1} collagen type I) at a cell concentration of 10^7 cells ml^{-1}, mixed with thrombin (0.5 U/ml) and immediately injected into a single stromal cell culture channel. The central channel and remaining stromal cell culture channel were filled with 2.5 mg ml^{-1} fibrin solution (0.15 U/ml aprotinin, 0.2 mg ml^{-1} collagen type I, 0.5 U/ml thrombin) and left to clot at room temperature for 5 min. After polymerization of the fibrin gel, EGM-2 medium was loaded into cell culture reservoirs and vacuum applied to fill medium channels. The device was incubated for 24 h at 37 °C and 5% CO$_2$ to allow any air bubbles on the gel–medium interface to dissipate and fibroblasts to become established within the fibrin gel matrix. HUVECs suspended in EGM-2 at a concentration of 5×10^6 cells ml^{-1} were introduced to the medium channel contralateral to the LF seeding, after removal of the medium from the corresponding medium reservoirs. The microfluidic chip was then tilted by 90 degrees and

incubated for 30 min, allowing HUVECs to adhere on the fibrin gel surface. Then the reservoirs were filled with EGM-2 and the chip kept in an incubator. In order not to disturb the gradient of LF-secreted factors, cell culture media were replaced only once after 3 days of co-culture by aspiration and refilling with fresh EGM-2 culture medium.

To observe the incorporation of pericytes during angiogenic sprout growth, human placenta pericytes (PromoCell) were resuspended with 2.5 mg ml^{-1} of a fibrinogen solution at a concentration of 5×10^5 cells ml^{-1}, and mixed with a thrombin solution to be injected into the central channel. For angiogenic sprouting in response to the cancer cells, U87MGs at a concentration of 10^7 cells ml^{-1} were used to be seeded contralaterally to the HUVECs in 2.5 mg ml^{-1} fibrin matrix. The rest of the experimental procedures were performed in the same way as in the angiogenesis experiments described above.

Measuring the success rate of vessel perfusion

To confirm whether the microvascular networks formed in our chip were perfusable, we used polystyrene beads of 7 μm diameter suspended in PBS solution. After 4 days of vasculogenic and angiogenic vessel formation, the reservoirs of each device were aspirated and the bead-suspending PBS solution was added on one side, allowing hydrodynamic forces to induce fluid flow through the microvascular networks. We checked whether the lumina at the interpost openings allowed the advective transport of beads, and counted the number of openings that were perfusable. We set out the criteria so that the microvascular networks where at least half of the openings allowed the passage of beads were determined as perfusable networks.

Immunostaining

Mouse monoclonal antibodies specific for human VE-cadherin (Alexa Fluor®488, clone 16B1) were purchased from eBioscience. Mouse monoclonal antibodies specific for ICAM-1 (Alexa Fluor®488, clone HCD54) and CD31 (Alexa Fluor®647, clone WM59) were purchased from BioLegend. Mouse monoclonal antibodies specific for human α-smooth muscle actin (α-SMA, Alexa Fluor®488, clone 1A4) and β-Catenin (Alexa Fluor®647, clone L54E2) were from R&D Systems and Cell Signaling, respectively. Rabbit polyclonal antibodies against human laminin and human collagen IV were purchased from Abcam. Mouse monoclonal antibody specific for human ZO-1 (Alexa Fluor®594, clone ZO1-1A12), Alexa Fluor®568 goat anti-rabbit IgG, Phalloidin (Alexa Fluor®488) and Hoechst 33342 were from Molecular Probes.

After washing cultures once with phosphate-buffered saline (PBS, Hyclone), cells were fixed in 4% (w/v) paraformaldehyde in PBS for 15 min, and then permeabilized using a 0.15% Triton X-100 (Sigma) in PBS solution for 15 min. After blocking using 3% bovine serum albumin (BSA, Sigma) in PBS for 1 h, samples were incubated overnight at 4 °C either with primary antibodies directly conjugated with fluorescent marker (VE-cadherin; 1 : 100, ICAM-1; 1 : 200, CD31; 1 : 200, α-SMA; 1 : 200, β-Catenin; 1 : 200, ZO-1; 1 : 100) or unconjugated antibodies (collagen IV; 1 : 100, laminin; 1 : 100), followed by incubation with fluorescence-conjugated secondary antibodies (1 : 1000, 4 h, 4 °C). For staining F-actin and DNA, Alexa

Fluor®488-Phalloidin (66 nM) and Hoechst 33342 (1 : 1000) were added to the chip for 1 h of incubation at room temperature. The samples were washed three times and stored in PBS before imaging. The EdU cell proliferation assay kit was purchased from Molecular Probes, and used according to the manufacturer's instructions.

Imaging

For cross-section and whole-construct imaging of 3D blood vessels, stained samples were examined using a FluoView FV1000 confocal laser scanning unit with the IX81 inverted microscope (Olympus) and images were captured with a confocal PMT detector. Lenses in use were x10, x20 and x40 (Olympus). Confocal images were processed by IMARIS software (Bitplane). A Phase-contrast (PhC) microscope (IX71; Olympus) or a differential interference contrast (DIC) microscope (IX81; Olympus) were used to perform visual microscopic observation and image acquisition of blood vessels.

Measurement of vessel permeability

The permeability coefficient of the blood vessels was quantified by introducing FITC-dextran (70 kDa, 10 μM, Sigma) into the microvascular networks derived from angiogenesis experiments, capturing time-sequential images of FITC-dextran diffusing through the endothelial barrier. After aspiration of the cell culture medium from the reservoirs on the chip, FITC-dextran solution was briefly added ($\sim$5 μl) at one fluidic channel to perfuse the intraluminal space, which was soon followed by the equilibrium of hydrostatic pressure between two fluidic channels. Fluorescence images were obtained every 5 s for 40 s with an IX81 inverted microscope (Olympus) and a CCD camera (Andor) using a $40\times$ objective. To minimize the compounding influences of complexities and randomness in the microvascular networks, we chose the region of a network where the segment of a blood vessel with a clear boundary between the endothelial wall and the extravascular fibrin matrix could be monitored exclusively in an optical window.

We calculated the permeability coefficient by using a method described elsewhere.[25] In brief, the permeability coefficient can be calculated as below assuming that the cross-sectional shape of the blood vessels is circular:

$$P = \frac{V}{S} \times \frac{dI/dt}{I_0}$$

where V and S are the total volume and surface area of the microvessels that fluorescent molecules have to pass to reach the perivascular region. I_0 is the intravascular intensity of FITC-dextran, dI/dt is the total fluorescence intensity change per unit time in the perivascular region. During the fluorescent imaging, the fluorescent intensity at the intravascular region (I_0) was not changed. The fluorescent images were analyzed with ImageJ (NIH).

Inflammatory response and HL-60 adhesion experiments

Microvascular networks derived from angiogenic sprouts at days 4–5 were stimulated for 4 h with 50 ng ml^{-1} of recombinant human TNF-α (PeproTech) or with 2 ng ml^{-1} of recombinant human IL-1α (PeproTech). Then these networks

were perfused with fresh EGM-2 medium, and labeled with CellTracker Red (5 µM, Molecular Probes) according to the manufacturer's instructions. Differentiated HL-60 cells were fluorescently labeled with CellTracker Green (5 µM, Molecular Probes), and then resuspended in fresh EGM-2 medium at a concentration of 1.5×10^6 cells ml^{-1}. To introduce the cells into the microvascular networks, all four reservoirs of the microfluidic chips were aspirated, and then 20 µl of the cell suspension loaded into a single inlet reservoir allowing the cells to flow into and adhere onto the apical surface of endothelium. The vascular networks were washed once with fresh EGM-2 to remove non-adherent cells, followed by filling the reservoirs with fresh EGM-2 medium.

Fluid perfusion experiments and statistical analysis of endothelial NO synthesis

The microfluidic chips designed for angiogenesis experiments were modified to enable constant medium flow to be introduced into the microvascular networks formed within a chip, as schematically presented in Fig. S1C, ESI†. Except for the flow-introducing serpentine channel network replacing the LO channel, the channel dimensions and experimental procedures for angiogenic sprouting were identical to those described in the above sections.

To estimate the flow rate that exerts a physiological level of shear stress, we assumed the microvascular networks as a multi-pipe system of parallel flow cases where each vessel has a circular cross-sectional shape and an identical length. According to our assumptions, the head loss of each vessel across the vascular network is identical, thus the flow rate at each blood vessel is calculated as follows:

$$h_f \propto \frac{Q_k}{A_k^2}$$

$$\frac{Q_1}{A_1^2} = \frac{Q_2}{A_2^2} = \cdots = \frac{Q_n}{A_n^2} = \frac{\sum_1^n Q_k}{A_1^2 + A_2^2 + \cdots + A_n^2}$$
$$= \frac{Q_{total}}{A_1^2 + A_2^2 + \cdots + A_n^2}$$

$$Q_k = Q_{total}\left(\frac{A_k^2}{A_1^2 + A_2^2 + \cdots + A_n^2}\right)$$

where h_f is the head loss across the microvascular network, Q_k is the volume flow rate at the k-th vessel, A_k is the cross-sectional area of the k-th vessel, and Q_{total} is the total volume flow rate which is the sum of the individual flows.

For a blood vessel with a diameter r and a volume flow rate Q, the shear stress can be calculated according to the following equation:

$$\tau = \frac{4Q\mu}{\pi r^3}$$

where μ is the viscosity of the perfusate, which is the cell culture medium having a viscosity value of 0.0008 Pa·s in our experiments.

From the confocal microscopic images of 7 microfluidic chips, we quantified the diameter of vessels along the

centerline of the microvascular networks. To match the physiological level of wall shear stress observed in venular microvessels *in vivo* (<10 dyne cm^{-2}), we determined the total volume flow rate for our microvascular networks (average vessel diameter of 35.7 ± 17.6 µm, s.d.) to be 300 µl h^{-1}, which is estimated to exert 0.31–7.22 dyne cm^{-2} (2.34 dyne cm^{-2} in average) of shear stress for each vessel depending on its diameter.

At day 5 of the sprouting angiogenesis process, the microvascular networks were perfused with the cell culture medium, EGM-2 *via* a syringe pump connected to an inlet of the microfluidic chip with the flow rate denoted above. Before each experiment, the microvascular networks were examined by microscopic observation to assess whether the vessel density and the diameter fit into the range of average values, and the vessels readily allowed fluid perfusion. In the experiments for quantifying the nitric oxide synthesis of the endothelial cells, the perfusates were supplemented with L-arginine (5 mM, Sigma) and DAF-FM DA (5 µM, Molecular Probes), to support and detect the NO synthesis of ECs.

After the fluid perfusion, the cytoskeleton reorganization and NO synthesis of ECs were accessed *via* confocal micrographs, using fluorescence signals derived from Alexa Fluor®488-Phalloidin and DAF-FM DA. Captured images were further analyzed with IMARIS (Bitplane). To quantify and compare NO synthesis between static and flow conditions from the images, the background fluorescence of each image was eliminated by subtracting the average intensity per pixel obtained from the regions where the vessels are absent. Z-projections of each 3D stack were collected *via* IMARIS, and ImageJ was used to obtain average intensity values for each pixel from the Z-projections. A one-tailed, unpaired Student's *t*-test was used to test for statistical significance between the groups.

Quantification of vessel area and length of sprouts

To quantify the vascular area coverage during vasculogenic blood vessel formation, cells were fluorescently labeled with CellTracker green, and fixed with 4% paraformaldehyde to be imaged by confocal microscope. Z-projections of the 3D stacks of microvascular networks were obtained each day with IMARIS (Bitplane), and further analyzed with ImageJ (NIH) to obtain binary images and calculate the proportion of the fluorescent pixels within the ROI of each image, deriving the vascular area coverage in the central channels for 4 days of vessel growth.

For the quantification of angiogenic sprout growth, DIC images of the central channel of each chip were obtained by Olympus IX81 microscope during 4 days of sprout growth. The lengths of the sprouts were determined by manually measuring distances between the original gel interface and the tip of each sprout.

Results

Microfluidic chip and experimental design

We fabricated the microfluidic chip using standard photolithography and soft lithography techniques. To complete the
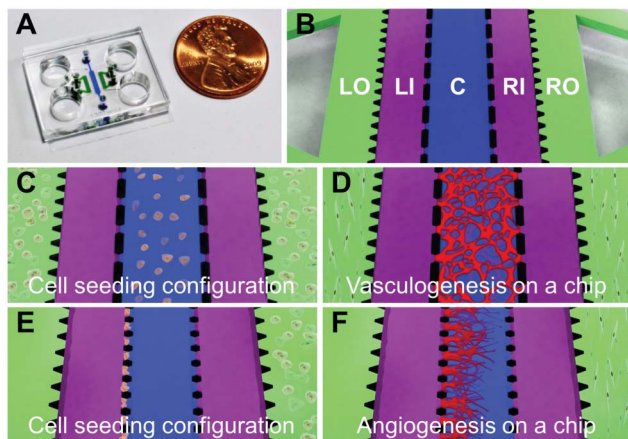
Fig. 1 Microfluidic chip design and cell seeding configurations for microvascular network and angiogenic sprout formation. (a) Photograph of the microfluidic chip, filled with colored fibrin matrix. (b) Schematic of the microfluidic channels partitioned by microposts. The central channel (C, blue) is flanked by two fluidic channels (Left Inside, LI, and Right Inside, RI, both colored purple) and two outside stromal cell culture channels (Left Outside, LO, and Right Outside, RO, both colored green). (c, d) Cell-seeding configuration for the vasculogenesis experiment. HUVECs are embedded in a 3D fibrin matrix placed in the central channel, and LFs with fibrin matrices are placed in the LO and RO channels. (e, f) Cell-seeding configuration for the angiogenesis experiment. HUVECs are coated on the side of central channel that is filled with acellular fibrin matrix. LFs in a fibrin matrix are placed in the RO channel.

chip, a molded piece of PDMS (polydimethylsiloxane) with embedded channel structures was bonded to a glass coverslip (Fig. 1A). The chip consists of five parallel channels: a central channel (C) and two stromal cell culture channels (LO, RO), separated by two fluidic channels (LI, RI) (Fig. 1B). The channels are partitioned by microposts whose geometry and dimensions are configured to allow the surface-tension-assisted patterning of ECM,[26] cells and culture medium into the designated microchannels. Spatially patterned co-culture of ECs (in C channel) and stromal cells (in LO or RO channels) supports diffusion-dependent, but contact-independent, heterotypic cell–cell communication, which allows the progression of two distinct processes of blood vessel formation, vasculogenesis and angiogenesis, to be replicated in a single versatile platform (Fig. 1C–F).

Using a common platform design, we optimized the dimensions of the central channel and the microposts for each blood vessel forming process (Fig. S1, ESI†). Vasculogenesis experiments were performed in chips with 1000 μm wide and 250 μm high central channels. Angiogenesis experiments were performed in chips with 700 μm wide and 100 μm high central channels. The openings between posts at the interface of the central channel and the fluidic channel serve as a route for the paracrine interactions between ECs and stromal cells during the vessel formation. These can also be used to access the intraluminal side of microvascular networks after the perfusion was established.

Formation of vasculogenesis- and angiogenesis-derived microvascular networks

We monitored the growth of the primary vessel network and angiogenic sprouts as it occurred over several days. We used human umbilical vein endothelial cells (HUVECs) as vascular precursor cells, and human normal lung fibroblasts (LFs) as stromal cells to support HUVEC morphogenesis via secretion of pro-angiogenic growth factors and extracellular matrix proteins.[27,28] To recreate highly pro-angiogenic ECM environments as found in wound healing and solid tumors,[29] we supplemented fibrin matrix with type I collagen (referred to simply as "fibrin matrix" hereafter) to form ECM constructs.

Vascular networks resembling primary plexus spontaneously emerged within the central channel (C) from HUVECs embedded in fibrin matrix, supported by soluble factors secreted by LFs cultured in separate flanking channels (LO, RO) (Fig. 1C). A day after seeding, HUVECs displayed elongated morphology with appearance of intracellular vacuoles (Fig. 2A). Assembly of HUVECs into tubule-like structures encompassing a nascent lumen was observed as early as day 2 (Fig. 2B). Further development of the vasculature resulted in interconnected networks occupying extended areas of fibrin matrix after 3 days (Fig. 2C). Perfusable microvascular networks that can be directly accessed via fluidic channels were established by day 4 to 5, followed by the enlargement of lumina (Fig. 2D). Initial cell density of HUVECs influenced the resulting vessel density as quantified in Fig. 2I.

We found that vasculogenic morphogenesis of HUVECs was dependent on the co-culture with LFs, since HUVECs without co-cultured LFs failed to form interconnected networks (Fig. S2A, ESI†). A mixed co-culture of HUVECs and LFs in the central channel also formed well-interconnected vascular networks after 5 days (Fig. S2B, ESI†). However, these networks were not connected to the medium channels (LI and LO) and could not be perfused (Fig. S2C, ESI†). This result was in sharp contrast to open networks when LFs were cultured in separate flanking channels (Fig. S2D, ESI†).

To induce angiogenic sprouting, we seeded HUVECs on the left side-wall of the acellular fibrin matrix that filled the central channel. LFs were positioned on the opposite side in the RO channel, exposing HUVECs to a gradient of LF-secreted factors (Fig. 1E). Within 24 h of co-culture, we observed robust formation of tip cells and angiogenic sprouts along the openings of the central channel (Fig. 2E). Once the sprouting had been initiated, the tip cells guided the growth of sprouts across the fibrin matrix until they reached the opposite end of the channel, as quantified in Fig. 2J. The growth of sprouts was supported by the proliferating cells at the stalk region showing sharp contrast with the non-proliferating tip cells (Fig. S3A, ESI†), which is in concordance with a previous study demonstrating distinct EC phenotypes during sprouting angiogenesis in vivo.[30] By day 2, endothelial cells comprising tubular structures were vacuolated (Fig. 2F). Defined lumina around the stalk region appeared by day 3 (Fig. 2G). The leading tip cells traversed the 700 μm wide central channel by day 4, after which they lost their filopoidal structures, and formed lumenized vessels to establish fluidic connections with the flanking medium channels (Fig. 2H and Movie S1†).
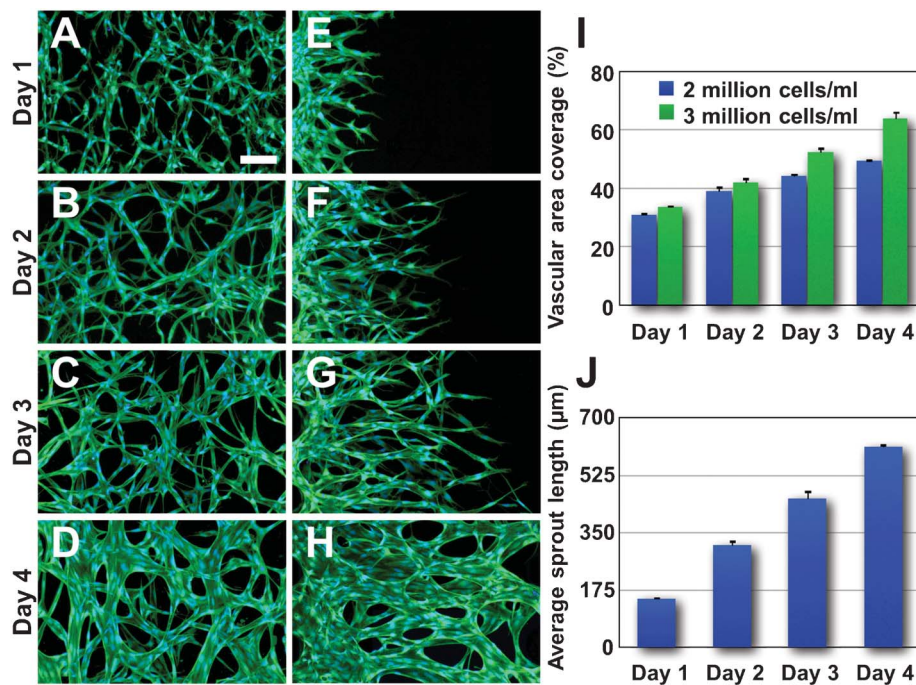
Fig. 2 Time-series micrographs of vasculogenic and angiogenic vessel formation in the fibrin matrix. Vasculogenesis: (a) day 1, HUVECs elongate and start to connect to each other. (b) Day 2, HUVECs start to form a network *via* a dynamic remodeling process, while nascent lumen structures appear. (c) By day 3, hollow lumina of HUVECs grow larger and merge to form well-interconnected tubular structures. (d) By day 4, a perfusable microvascular network is established as the luminal sides of the vessels are connected to the medium channels. Angiogenesis: (e) within 24 h after attaching HUVECs to fibrin walls in the central channel, endothelial sprouts with tip cells appear along the central fibrin matrix. (f) By day 2, vacuole formation starts in stalk regions. The sprouts continue to extend across the middle channel. (g) By day 3, defined lumina can be observed within the sprouts. (h) By day 4, growing angiogenic sprouts traverse across the entire width of the 700 μm central channel, establishing perfusion through luminal access with the RI medium channel. Cells were labeled with CellTracker green and fixed and stained for nuclei (blue). (i) Quantification of vasculogenic vessel network growth by total vascular covered area in *z*-projected image (*n* = 6 chips per day per condition). (j) Quantification of angiogenic sprout growth by tip cell distance from the left side of fibrin matrix (*n* = 5 chips for day 1, 2, 3 and *n* = 4 chips for day 4). Scale bar, 100 μm; error bars represent SEM.

Culturing HUVECs without LFs or seeding LFs ipsilateral (LO channel) to HUVECs failed to induce robust angiogenic sprout formation and growth (Fig. S3B, C, ESI†), indicating that angiogenic sprouting requires an appropriate directional gradient of pro-angiogenic factors secreted by LFs.

To test whether soluble VEGF directs angiogenic sprouting in our chip, we applied gradients of VEGF (0–50 ng ml^{-1}) across the fibrin matrix. This treatment induced initial steps of angiogenic sprouting as shown by robust tip cell formation, but the sustained length extension and lumenization of sprouts was not as evident as with LF-induced sprouting (Fig. S3D, ESI†).

Morphological and biochemical characterization of the vessels

To test whether the engineered blood vessels exhibit physiological characteristics, we tested the vessels for their 3D structural integrity and the presence of characteristic marker proteins of intact blood vessels. Immunofluorescence micrographs of the microvascular network formed through vasculogenesis (Fig. 3A) and angiogenesis (Fig. 3B) exhibited the complex inter-connectiveness and bifurcated architecture found in native vasculatures. Micrographs of angiogenic sprouts grown for 2 days (Fig. 3C) with a high magnification image of angiogenic tip cells (Fig. 3D) clearly display a

characteristic migratory morphology with multiple filopodia extensions at the sprouting fronts. Moreover, cross-sectional images of blood vessels (Fig. 3E and Fig. S4A, B, ESI†) showed the presence of a continuous, hollow lumen along the length of the vessels, enclosed by ECs. We also found continuous cell–cell junctions lining the intersection of the endothelial cells, as shown by the presence of the adherens junction proteins, VE-Cadherin and β-catenin, and tight junction protein, ZO-1 (Fig. 3F and Fig. S5, ESI†). Notably, these endothelial cells display the morphological features of venular microvessels found *in vivo*,[31] such as an elongated morphology aligned with the longitudinal direction of capillary-like structures. This is in sharp contrast to the randomly-aligned morphology exhibited by EC monolayers grown on 2D substrates, or ECs comprising endothelialized 3D hydrogel channels.[10,12,14]

We then analyzed the cells for signs of vessel maturation. First, using immunofluorescence to detect the apical expression of TNF-α-induced ICAM-1 and the basal deposition of collagen IV, we confirmed the appropriate apical–basal polarity of the endothelium (Fig. 3G). Through the vessels stained for laminin and collagen IV, we also observed the deposition of basement membrane by endothelial cells around the perivascular extracellular matrix, a sign of vessel matura-
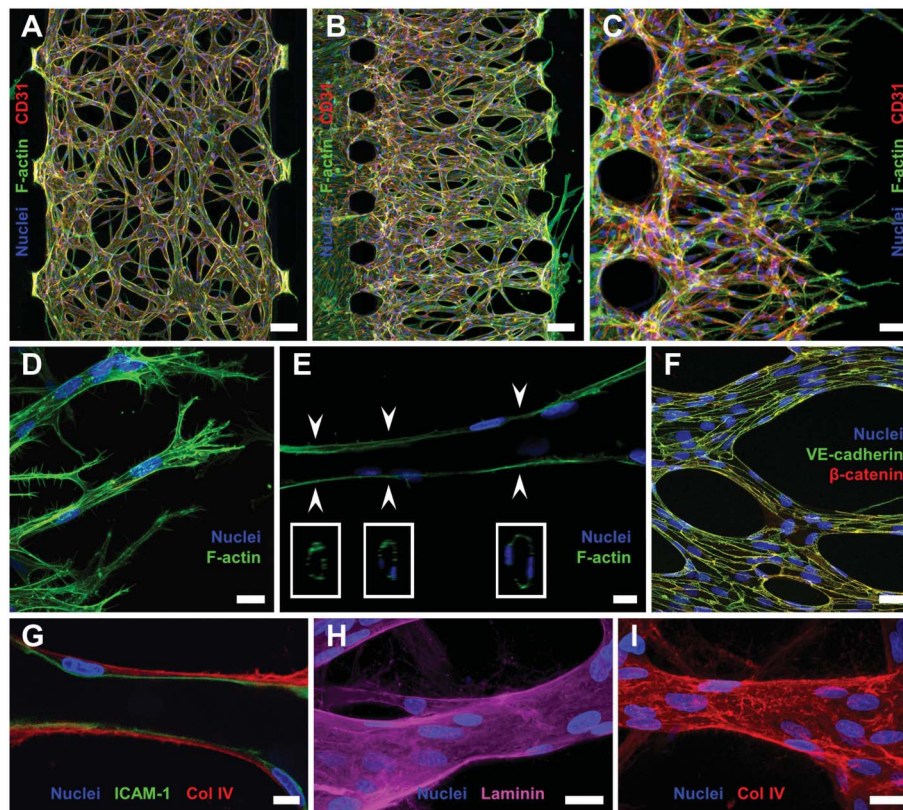
Fig. 3 Engineered 3D microvessels characterized by immunofluorescence. (a–b) Confocal micrographs showing the overall architectures of vascular networks established by (a) vasculogenic and (b) angiogenic processes at day 4. Scale bars, 100 μm. (c) Angiogenic sprouts grown for 2 days. Scale bar, 50 μm. (d) Higher magnification image shows the F-actin-rich filopodia extensions of angiogenic tip cells. Scale bar, 20 μm. (e) Cross-sectional images of a blood vessel showing a hollow lumen enclosed by ECs. Scale bar, 10 μm. (f) Microvascular network immunostained against adherens junction proteins, VE-cadherin (green) and β-catenin (red). Scale bar, 50 μm. (g) Longitudinal cross-section of a TNF-α-stimulated blood vessel stained for ICAM-1 (green) and collagen IV (red). Scale bar, 10 μm. (h, i) Confocal micrographs of vessels stained for the major components of basement membrane, laminin (purple) or collagen IV (red). Scale bars, 20 μm.

tion associated with mural cell association and vascular stabilization[32] (Fig. 3H and I).

Perfusable and intact lumina of the engineered microvascular networks

We next tested whether the microvascular networks grown in the microfluidic chip provide 3D intact perfusable vessels with the practical potential to investigate flow-mediated endothelial mechanotransduction, vascular barrier function and endothelium–leukocyte interactions.

To demonstrate the direct fluid interconnection between the medium channels and the endothelial lumina, we introduced solutions containing fluorescent polystyrene microbeads into the microvascular networks along with the luminal flow induced by hydrostatic pressure differential. A minute volume difference in the reservoirs (~20 μl) established fluid flow through the vessels in the central channel, allowing the passage of 7 μm polystyrene beads, whose dimension is comparable to the blood-borne cell types (Fig. 4A and Movies S2, 3†). As visualized by the movement of the tracer beads, the microvascular networks allowed fluid flow through the lumina without bead infiltration into the abluminal fibrin matrix. Solutions containing FITC-dextran (70 kDa) were also introduced into the vessels that were labeled with CellTracker red

(Fig. 4B), exhibiting clear retention of FITC-dextran inside the vessels without uncontrolled leakage into perivascular space. Quantitative assessment of angiogenesis-derived blood vessels revealed that the permeability coefficient of 70 kDa FITC-dextran through the endothelial walls measured to be $(1.70 \pm 0.36) \times 10^{-6}$ cm s^{-1} ($n = 3$) at 4–5 days. This permeability coefficient illustrated an intact, stronger barrier function of our vessels, which is closer to that of *in vivo* venular vessels,[33] when compared to the other *in vitro* vessels reported previously.[10,14,34]

To test the robustness of our method, we quantified the success rate of perfusable network formation by flowing microbeads through the lumina of blood vessels. We found that 88% ($n = 36$ chips, 4 trials) and 91% ($n = 36$ chips, 4 trials) chips successfully established perfusable networks *via* vasculogenic and angiogenic processes, respectively. Within the successful devices, the percentages of interpost regions encompassing the openings were 62% and 70% for the vasculogenic and angiogenic process. These microvascular networks maintained patent and perfusable lumina for at least an additional 7 days without discernible regression or destabilization (Fig. S6A, B, ESI†).
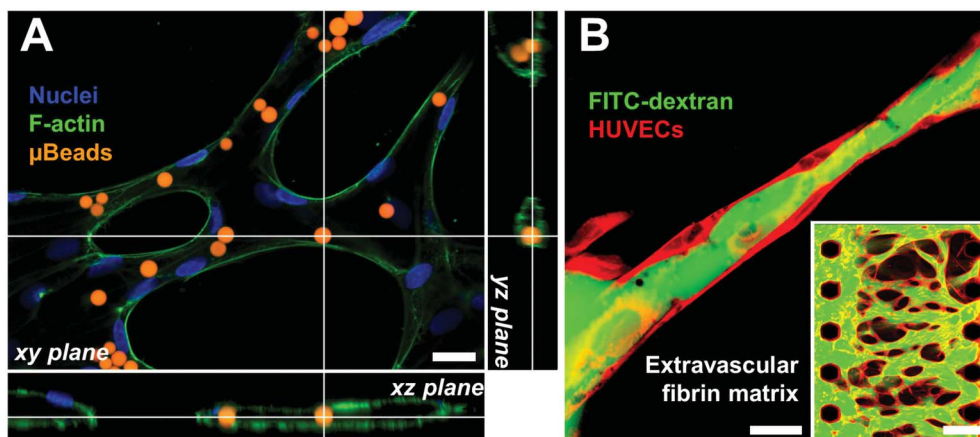
Fig. 4 Introduction of solutions containing microbeads or fluorescent dye into the perfusable microvessels. (a) Red fluorescent microbeads (7 μm, red) introduced into the microvascular network exclusively localize within the luminal space of F-actin-labeled endothelium (green). (b) Intravascular introduction of FITC-dextran (70 kDa, green) into the blood vessel labeled with CellTracker red. Scale bar, 20 μm. Inset scale bar, 200 μm.

Flow-induced endothelial responses

As an innermost cellular layer of blood vessels, the endothelium is constantly exposed to mechanical stimuli exerted by blood flow. Rather than being passive pipelines, blood vessels faithfully respond to the mechanical stimuli, contributing to the structural integrity and normal functions of blood vessels, and in turn, abnormal blood flow or vessel occlusion leads to the pathogenesis of diverse diseases.[35,36]

To examine whether constant fluid flow through the *in vitro* 3D blood vessels evokes endothelial responses and functional upregulation, we examined the cytoskeleton reorganization of ECs and nitric oxide (NO) synthesis in response to fluid flow. To estimate the flow rate necessary to approximately match the physiological level of shear stress (1 to 10 dyne/cm^2 in venular microvessels[37]), we considered the range of diameters of blood vessels derived from the angiogenesis experiments (35.7 $\pm$ 17.6 μm, s.d, 87 vessels from 7 chips, Fig. S7, ESI†). The volume flow rate for the entire vessel network was 300 μl h^{-1}, which established the range of shear stress at approximately 0.31–7.22 dyne/cm^2, depending on the size of each microvessel. For long-term perfusion of the microvessels with constant volumetric flow rate, the chip design was modified to have a fluidic inlet and serpentine channel network replacing the LO channel (Fig. S1C, ESI†).

We found that under such conditions, fluid flow induced cytoskeleton reorganization of the ECs comprising the microvascular networks which showed distinct distribution of F-actin microfilaments compared to static conditions. In the absence of fluid flow, dense F-actin bundles preferentially localized at the periphery of endothelial cells where the cell–cell contacts were present (Fig. 5A). In contrast, ECs exposed to fluid flow for 2 h displayed evenly distributed stress fibers that are parallel and aligned in the direction of the fluid flow. The peripheral band seen in static conditions was not discernible (Fig. 5B).

We next examined the effect of fluid flow in the functional upregulation of blood vessels through the synthesis of nitric oxide, a crucial and multifunctional signaling molecule for vascular physiology. Flow-mediated shear stress is a key determinant of activation of endothelial NO synthesis,[38] which exerts a wide range of effects including modulation of blood flow, anti-thrombotic, anti-inflammatory and anti-proliferative functions.[39] To examine the effect of fluid flow in activation of endothelial NO synthesis in our chip, we perfused angiogenesis-derived microvascular networks with cell culture medium adding L-arginine as a precursor for NO synthesis (5 mM), and the NO-reactive fluorescent dye DAF-FM DA (5 μM). Under static conditions, the endothelial synthesis of nitric oxide induced only a low level fluorescence signal even in the presence of high concentrations of L-arginine (5 mM), a physiological precursor for the NO synthesis (Fig. 5C). However, microvascular networks perfused for only one hour exhibited a significant increase in the NO-reactive fluorescence signal, sufficient to observe the outline of the endothelium (Fig. 5D and E). We also observed that flow-mediated upregulation of NO synthesis required exogenous L-arginine in the perfusate,[40] as perfusion of the medium without a L-arginine supplement did not increase the endothelial NO synthesis compared with static conditions (Fig. S8, ESI†).

In vitro modeling of endothelial interactions with pericytes, cancer cells and leukocytes

Endothelial cells receive and integrate diverse signals from nearby microenvironments and other cell types to accommodate tissue-specific functions or to control angiogenic switch.[41–43] To investigate whether our chip can reproduce vessel growth and responses *via* interactions with diverse cell types, we performed co-culture experiments with pericytes and cancer cells.

To simulate pericyte recruitment from interstitial tissue toward newly formed angiogenic sprouts, we incorporated human placenta pericytes in the fibrin matrix filling the central channel, whereby LF-induced angiogenic sprouts extended across the ECM embedding the pericytes. The presence of pericytes in the central channel did not disturb the growth of angiogenic sprouts to form perfusable micro-
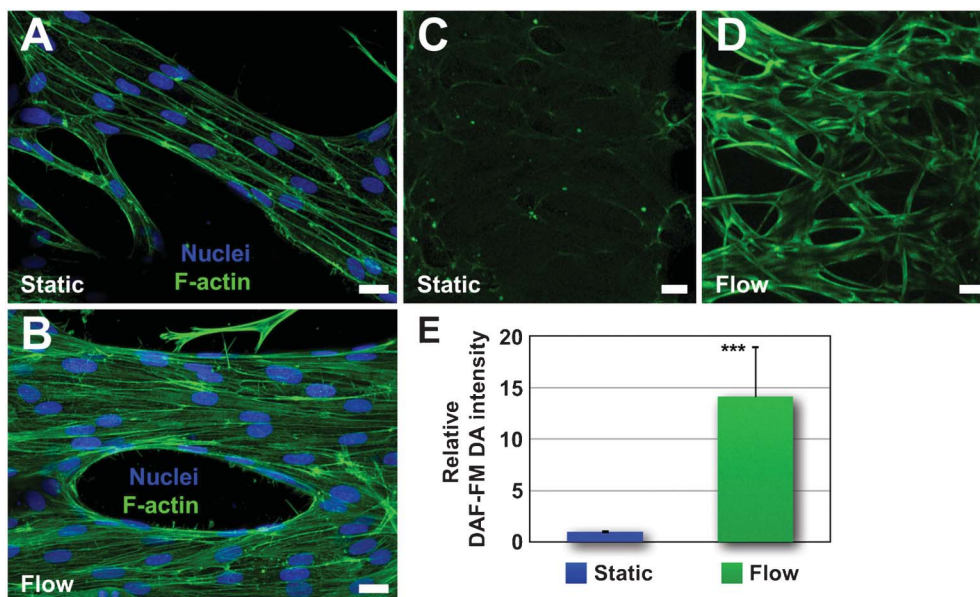
Fig. 5 Endothelial cell responses to luminal fluid flow. (a) F-actin (green) distribution of ECs under static conditions. Scale bar, 20 μm. (b) Changes in F-actin distribution in response to luminal flow for 2 h. Scale bar, 20 μm. (c) Endothelial NO synthesis under static conditions assayed by DAF-FM DA fluorescence dye (green). Scale bar, 50 μm. (d) Significant increase in fluorescent intensity of DAF-FM DA after exposure to 1 h of luminal flow. Scale bar, 50 μm. (e) Quantitative analysis of the fluorescence intensity showing a 14-fold increase after flow exposure, compared to static conditions ($n = 9$ for static, $n = 7$ for flow condition, ***$p < 0.005$). Error bars represent SEM.

vascular networks, both in the timescale of sprout length extension and the establishment of perfusable lumina (~88%, $n = 33$ chips, 3 trials). By day 4, pericytes expressing α-smooth muscle actin (α-SMA) were frequently found adjacent to the blood vessels with stretched morphology to cover abluminal surface of the endothelium (Fig. 6A). A high magnification image and the corresponding confocal sections showed pericytes attached to the endothelial-derived collagen IV basement membrane (Fig. 6B).

We then explored whether, in our chip-based microvasculature, cancer cell-secreted factors support the initiation and growth of angiogenic sprouts. We co-cultured HUVECs with highly malignant human glioblastoma multiforme cells, U87MG, seeded in the stromal cell culture channel (RO). We found that within 24 h of co-culture, HUVECs invaded the fibrin matrix apparently in response to the U87MG-derived factors. Whereas the sustained outgrowth of sprouts exhibited similar length extension (day 2: 341.0 ± 18.7 μm, day 4: 620.3 ± 5.2 μm, mean of average sprout length from 4 chips per day, error represents SEM) compared to LF-mediated sprouting experiments, these sprouts displayed aberrant morphology. At day 2, the angiogenic sprouts showed frequent branching of the immature tubules, as shown by multiple tip cells at the distal edges of sprouts (Fig. 6C). And rather than growing directionally toward U87MG cells, some sprouts were convoluted and aberrantly fused with adjacent vessels resembling the vasculatures of corresponding *in vivo* scenarios.[44] When compared to LF-induced sprouts, U87MG-induced sprouts exhibit inefficient formation of perfusable vascular networks at day 4, frequently encompassing immature and poorly lumenized vessels (Fig. 6D).

The interactions between the endothelium and white blood cells play a central role in immunity,[45] which prompted us to examine whether the microvascular networks exhibit appropriate functions in the presence of pro-inflammatory cytokines. We therefore tested, in our system, endothelial responses and leukocyte adhesion after stimulation by inflammatory cytokines. The endothelium expressed a leukocyte adhesion protein, ICAM-1, on the apical surface in response to tumor necrosis factor-α (TNF-α, 50 ng ml^{-1}) or interleukin-1α (IL-1α, 2 ng ml^{-1}) (Fig. 6E). The endothelium stimulated with TNF-α promoted the adhesion of differentiated HL-60 cells which were introduced along with the transient luminal flow. Upon arrest, the HL-60 cells adopted a flattened morphology and actively crawled on the apical surface of the endothelium (Fig. 6F and Movie S4†), simulating the adhesive interactions between leukocytes and the endothelium found in inflammatory responses.

Discussion

Despite the significant progress, it has not yet been possible to reconstitute the characteristic functions and responses of blood vessels with their natural 3D architectures. The artifacts shown in the previous studies mainly stem from their limited ability to combine physiological vessel forming processes and luminal flow which contribute typical structural and functional features of blood vessels. While recent studies have demonstrated the feasibility to achieve perfusable blood vessels by mimicking physiological angiogenic processes,[19,23] these methods still depend on the artificial structural guides
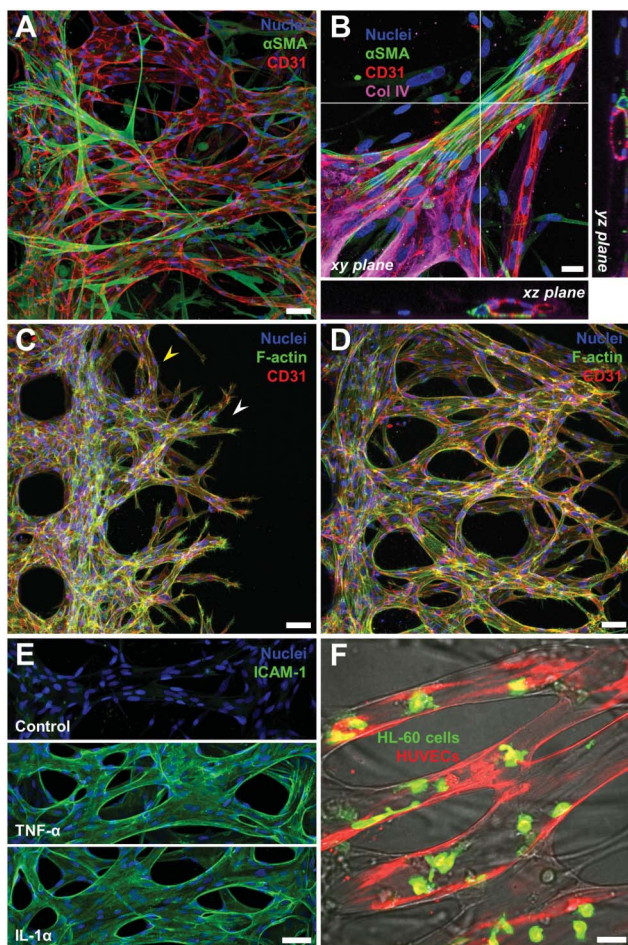
Fig. 6 Endothelial cell interactions with pericytes, cancer cells and leukocytes. (a) Microvascular network (CD31, red) covered with pericytes (α-SMA, green). Scale bar, 50 μm. (b) Higher magnification image and corresponding confocal sections of a pericyte-decorated blood vessel. Scale bar, 20 μm. (c, d) Confocal micrographs of angiogenic sprouts grown for 2 and 4 days under co-culture with U87MG cancer cells, characterized by the sprouts with branching tip cells (white arrowhead) and convoluted and aberrantly fused tubules (yellow arrowhead). Scale bars, 20 μm. (e) Expression of ICAM-1 (green) on the apical surface of blood vessels in response to inflammatory cytokines TNF-α (50 ng ml^{-1}) or IL-1α (2 ng ml^{-1}). Scale bar, 50 μm. (f) Adhesion of activated HL-60 neutrophils (green) on the inner surface of endothelium (red) promoted by endothelial stimulation with TNF-α. Scale bar, 20 μm.

in shaping outlines of the vasculatures. Furthermore the behaviors of endothelial cells observed in these methods were deviated from those shown in actual vasculogenesis and angiogenesis processes, leading to compromised vascular functions. In particular, the integrity of barrier function and mechanosensitive responses should be confirmed to further exploit 3D blood vessel models in the investigations of transendothelial migration or endothelial mechanotransduction which still rely on 2D endothelial monolayers. The method presented in this study conveys key advantages as it not only closely mimics endothelial morphogenesis processes to form intact, perfusable microvascular networks, but also

recreates important vessel-specific functions defined by luminal flow.

Our spatially patterned co-culture approach provides a reliable mimicry of a living system, whereby tightly coordinated crosstalk between ECs and perivascular or stromal cell types precisely control the formation and function of blood vessels. In accordance with earlier *in vivo* and *in vitro* studies,[24,46] we demonstrated that the multistep cascade of the angiogenic process cannot be fully reproduced by addition of a potent pro-angiogenic factor, such as VEGF, on the monoculture of endothelial cells, whereas EC–fibroblast interaction robustly induced lumenized vessel formation. Moreover, the versatile capabilities of our patterned co-culture approach allowed diverse types of cell–cell interactions to be modeled in a single platform, which effectively reproduced tumor-induced angiogenesis (in the co-culture of ECs and U87MG cells) as well as endothelial–pericyte interactions (in the tri-culture of ECs, fibroblasts and pericytes). The cellular compositions in the culture can be further flexibly configured to confer increased biological relevance as well as organ- and microenvironment-specific characteristics to the vessels.

The exact mechanisms by which growing tubules form accessible inlets at the ECM–fluid interface remain unclear and require further investigation. However, we speculate that the chemotactic gradient of fibroblast-secreted factors drives spontaneous anastomotic fusion observed in our chip. In our results, both vasculogenic and angiogenic processes require LF-secreted factors. In contrast to the angiogenic sprouting, vasculogenic processes do not necessarily require LF-secreted factors to be present in a form of concentration gradient. However, interestingly, a mixed co-culture of ECs and fibroblasts resulted in well-interconnected but non-perfusable (or poorly perfusable at best) vascular networks, where the tubules rarely extended toward the ECM-fluid interfaces at the apertures (Fig. S2, ESI†). Although we do not suggest mechanisms underlying this observation as well as relevant *in vivo* phenomenon, spontaneous formation of open lumina by growing endothelial tubules provide a novel methodology to establish perfusable vasculatures in a 3D cell culture system.

The processes of new blood vessel formation require the establishment of functional vascular loop to prompt the survival and stabilization of newly formed vessels,[47] as well as physiological function and homeostasis.[48] Not only were the microvascular networks formed in our chip patent and durable, they also responded faithfully to the fluid flow displaying cytoskeleton reorganization and activation of NO synthesis. Considering multifunctional vascular regulations of NO, enhanced NO production suggests that the mechanical forces exerted by the fluid flow contribute as determinants to the functional behaviors of our endothelium as in the coincidence with living vasculatures transmitting the fluid. Notably, flow-mediated F-actin reorganization of ECs was observed even briefly after 2 h of fluid perfusion. Whereas the reorientation of cell bodies into the fluid direction precedes the F-actin reorganization in endothelial monolayers on 2D substrates,[49] ECs forming 3D microvessels in our chip

displayed well-aligned cellular patterns along the longitudinal axis of the tubules, even in a static, pre-sheared condition, which might contribute to our observations.

The vasculatures formed in our chip displayed intact barrier function as well as long-term stability. These attributes provide benefits for the investigation of how vascular integrity can be either augmented or compromised in response to microenvironmental cues. Examples would include the presence of physiological flow and pericyte coverage for their regulations in the vascular physiology/homeostasis. Our system also allows the study of microvascular occlusion and hyper-permeability observed during diverse diseases such as cancer, infection with malaria and diabetic retinopathy, to name a few.

Conclusions

Given the primary functions of blood vessels as mechanosensitive and selective barrier between flowing blood compounds and interstitial tissues, there is a pressing need for a robust and practical approach that can combine physiological formation of 3D blood vessels with perfusable and stable lumina, whereby key microenvironmental factors can be integrated within an *in vitro* model that more closely resembles the *in vivo* state of tubular vessels transmitting fluid flow.

Here we report a robust experimental platform for studying the formation and function of 3D blood vessels in response to critical microenvironmental factors. Our microfluidic chip employs spatially controlled co-cultures of blood vessel-relevant cell types, which comes closer to reconstituting the heterotypic cell–cell interactions found in healthy and pathologic scenarios. A major advance of our approach is the ability to grow perfusable microvascular networks that are similar in 3D architectures, intact barrier function, long term stability and salient biochemical markers to their *in vivo* counterparts. This unique feature distinguishes our method from previously reported microtechnology-assisted perfusable blood vessel models, which are usually based on endothelialization of preformed hydrogel templates,[10,14,50] or limited reconstitution of endothelial morphogenesis.[19,20,23] The perfusable microvessels allow further functional and structural modulations in response to biochemical and biophysical cues, and can be adapted to design unique *in vitro* models to investigate vascular barrier function, transendothelial migration of blood circulating cells, and endothelial mechanotransduction in close similarities with living systems. In addition, formation of blood vessels can involve a variety of other perivascular cell types or endothelial cells from different origins to recreate vascular microenvironments found in the blood–brain barrier, stem cell niches, and tumor metastases.

The robustness and reproducibility of our chip-based microvessels, combined with the feasibility for flexibly customizing the chip design, promise to make it a versatile platform for the fundamental study of vascular biology and vascularized micro-organs or human disease models for drug discovery.

Acknowledgements

References

1 P. Carmeliet and R. K. Jain, *Nat. Rev. Drug Discovery*, 2011, **10**, 417–427.

2 J. Gavard and J. S. Gutkind, *Nat. Cell Biol.*, 2006, **8**, 1223–1234.

3 E. Tzima, M. Irani-Tehrani, W. B. Kiosses, E. Dejana, D. A. Schultz, B. Engelhardt, G. Cao, H. DeLisser and M. A. Schwartz, *Nature*, 2005, **437**, 426–431.

4 C. V. Carman and T. A. Springer, *J. Cell Biol.*, 2004, **167**, 377–388.

5 P. L. Tremblay, J. Huot and F. A. Auger, *Cancer Res.*, 2008, **68**, 5167–5176.

6 D. E. Ingber, *Circ. Res.*, 2002, **91**, 877–887.

7 E. W. Raines, *Int. J. Exp. Pathol.*, 2001, **81**, 173–182.

8 D. E. Ingber and J. Folkman, *Cell*, 1989, **58**, 803–805.

9 D. G. Stupack and D. A. Cheresh, *Science's STKE*, 2002, **2002**, pe7.

10 K. M. Chrobak, D. R. Potter and J. Tien, *Microvasc. Res.*, 2006, **71**, 185–196.

11 S. Chung, R. Sudo, P. J. Mack, C. R. Wan, V. Vickerman and R. D. Kamm, *Lab Chip*, 2009, **9**, 269–275.

12 G. M. Price, K. H. K. Wong, J. G. Truslow, A. D. Leung, C. Acharya and J. Tien, *Biomaterials*, 2010, **31**, 6182–6189.

13 J. W. Song and L. L. Munn, *Proc. Natl. Acad. Sci. U. S. A.*, 2011, **108**, 15342–15347.

14 Y. Zheng, J. Chen, M. Craven, N. W. Choi, S. Totorica, A. Diaz-Santana, P. Kermani, B. Hempstead, C. Fischbach-Teschl and J. A. López, *Proc. Natl. Acad. Sci. U. S. A.*, 2012, **109**, 9342–9347.

15 I. K. Zervantonakis, S. K. Hughes-Alford, J. L. Charest, J. S. Condeelis, F. B. Gertler and R. D. Kamm, *Proc. Natl. Acad. Sci. U. S. A.*, 2012, **109**, 13515–13520.

16 M. Tsai, A. Kita, J. Leach, R. Rounsevell, J. N. Huang, J. Moake, R. E. Ware, D. A. Fletcher and W. A. Lam, *J. Clin. Invest.*, 2012, **122**, 408–418.

17 K. H. K. Wong, J. M. Chan, R. D. Kamm and J. Tien, *Annu. Rev. Biomed. Eng.*, 2012, **14**, 205–230.

18 V. Vickerman, J. Blundo, S. Chung and R. Kamm, *Lab Chip*, 2008, **8**, 1468–1477.

19 J. H. Yeon, H. R. Ryu, M. Chung, Q. P. Hu and N. L. Jeon, *Lab Chip*, 2012, **12**, 2815–2822.

20 J. W. Song, D. Bazou and L. L. Munn, *Integr. Biol.*, 2012, **4**, 857–862.

21 M. P. Cuchiara, D. J. Gould, M. K. McHale, M. E. Dickinson and J. L. West, *Adv. Funct. Mater.*, 2012, **22**, 4511–4518.

22 B. Carrion, C. P. Huang, C. M. Ghajar, S. Kachgal, E. Kniazeva, N. L. Jeon and A. J. Putnam, *Biotechnol. Bioeng.*, 2010, **107**, 1020–1028.

23 J. M. Chan, I. K. Zervantonakis, T. Rimchala, W. J. Polacheck, J. Whisler and R. D. Kamm, *PLoS One*, 2012, **7**, e50582.

24 A. C. Newman, M. N. Nakatsu, W. Chou, P. D. Gershon and C. C. W. Hughes, *Mol. Biol. Cell*, 2011, **22**, 3791–3800.

25 X. Zhou, B. Chen, P. J. Hoopes, T. Hasan and B. W. Pogue, *Radiat. Res.*, 2009, **168**, 299–307.

26 C. P. Huang, J. Lu, H. Seon, A. P. Lee, L. A. Flanagan, H. Y. Kim, A. J. Putnam and N. L. Jeon, *Lab Chip*, 2009, **9**, 1740–1748.

27 M. N. Nakatsu, R. C. A. Sainson, J. N. Aoto, K. L. Taylor, M. Aitkenhead, S. Perez-del-Pulgar, P. M. Carpenter and C. C. W. Hughes, *Microvasc. Res.*, 2003, **66**, 102–112.

28 X. Chen, A. S. Aledia, C. M. Ghajar, C. K. Griffith, A. J. Putnam, C. C. W. Hughes and S. C. George, *Tissue Eng. A*, 2008, **15**, 1363–1371.

29 H. Dvorak, V. Harvey, P. Estrella, L. Brown, J. McDonagh and A. Dvorak, *Lab. Invest.*, 1987, **57**, 673–686.

30 H. Gerhardt, M. Golding, M. Fruttiger, C. Ruhrberg, A. Lundkvist, A. Abramsson, M. Jeltsch, C. Mitchell, K. Alitalo and D. Shima, *J. Cell Biol.*, 2003, **161**, 1163–1677.

31 P. He and R. Adamson, *Microcirculation*, 1995, **2**, 267–276.

32 G. E. Davis and D. R. Senger, *Circ. Res.*, 2005, **97**, 1093–1107.

33 W. Yuan, Y. Lv, M. Zeng and B. M. Fu, *Microvasc. Res.*, 2009, **77**, 166–173.

34 V. Vickerman and R. Kamm, *Integr. Biol.*, 2012, **4**, 863–874.

35 H. H. Lipowsky, *Microcirculation*, 2005, **12**, 5–15.

36 C. Hahn and M. A. Schwartz, *Nat. Rev. Mol. Cell Biol.*, 2009, **10**, 53–62.

37 S. Sheikh, G. E. Rainger, Z. Gale, M. Rahman and G. B. Nash, *Blood*, 2003, **102**, 2828–2834.

38 S. Dimmeler, I. Fleming, B. Fisslthaler, C. Hermann, R. Busse and A. M. Zeiher, *Nature*, 1999, **399**, 601–605.

39 P. Pacher, J. S. Beckman and L. Liaudet, *Physiol. Rev.*, 2007, **87**, 315–424.

40 M. S. Joshi, T. B. Ferguson, F. K. Johnson, R. A. Johnson, S. Parthasarathy and J. R. Lancaster, *Proc. Natl. Acad. Sci. U. S. A.*, 2007, **104**, 9982–9987.

41 A. Armulik, A. Abramsson and C. Betsholtz, *Circ. Res.*, 2005, **97**, 512–523.

42 R. S. Kerbel, *N. Engl. J. Med.*, 2008, **358**, 2039–2049.

43 N. J. Abbott, L. Rönnbäck and E. Hansson, *Nat. Rev. Neurosci.*, 2006, **7**, 41–53.

44 M. Papetti and I. M. Herman, *Am. J. Physiol. Cell Physiol.*, 2002, **282**, C947–C970.

45 T. M. Carlos and J. M. Harlan, *Blood*, 1994, **84**, 2068–2101.

46 A. Alajati, A. M. Laib, H. Weber, A. M. Boos, A. Bartol, K. Ikenberg, T. Korff, H. Zentgraf, C. Obodozie and R. Graeser, *Nat. Methods*, 2008, **5**, 439–445.

47 R. J. Dekker, R. A. Boon, M. G. Rondaij, A. Kragt, O. L. Volger, Y. W. Elderkamp, J. C. M. Meijers, J. Voorberg, H. Pannekoek and A. J. G. Horrevoets, *Blood*, 2006, **107**, 4354–4363.

48 S. Chien, *Am. J. Physiol.: Heart Circ. Physiol.*, 2007, **292**, H1209–H1224.

49 C. Galbraith, R. Skalak and S. Chien, *Cell Motil. Cytoskeleton*, 1998, **40**, 317–330.

50 J. S. Miller, K. R. Stevens, M. T. Yang, B. M. Baker, D. H. T. Nguyen, D. M. Cohen, E. Toro, A. A. Chen, P. A. Galie and X. Yu, *Nat. Mater.*, 2012, **11**, 768–774.